Theoretical Study of a Membrane Reactor for the Water Gas Shift Reaction Under Nonisothermal Conditions

María E. Adrover, Eduardo López, Daniel O. Borio, and Marisa N. Pedernera
Dept. of Chemical Engineering-Universidad Nacional del Sur-PLAPIQUI,
CONICET, Camino La Carrindanga Km 7, Bahía Blanca, Argentina

DOI 10.1002/aic.11929
Published online August 13, 2009 in Wiley InterScience (www.interscience.wiley.com).

A simulation of a membrane reactor for the water gas shift reaction is carried out by means of a 1D pseudo-homogeneous nonisothermal mathematical model. The composite membrane consists of a dense layer of Pd (selective to H_2) supported over a porous ceramic layer. The effect of temperature, overall heat-transfer coefficient, and mode of operation on the membrane reactor performance and stability are analyzed, and the results obtained are compared with those corresponding to a reactor with no hydrogen permeation. © 2009 American Institute of Chemical Engineers *AIChE J,* 55: 3206–3213, 2009

Keywords: membrane reactors, water gas shift, Pd membrane, thermal effects

Introduction

Most of the hydrogen is produced industrially by steam reforming of hydrocarbons or alcohols (e.g., for fuel cell applications). The process gas stream leaving the steam reformer is composed of H_2, CO, CO_2, H_2O, and small amounts of unconverted reactant (CH_4). Usually, the CO concentration of this stream must be reduced up to a specified level, with two main goals: (1) to increase the H_2 production rate and (2) to purify the process stream. To these ends, the water gas shift reaction (WGSR) is widely used:

$$CO + H_2O \Leftrightarrow CO_2 + H_2 \quad \Delta H^{\circ}_{298\,K} = -41.09\,kJ/mol \quad (1)$$

Reaction (1) is moderately exothermic and strongly controlled by the chemical equilibrium, which is favored at low temperatures. In small-scale processes, such as the fuel processing for fuel cells (e.g., PEM cells) normally the WGSR is carried out in a single reactor at an intermediate temperature level.[1]

An interesting alternative for increasing the CO conversion is the membrane reactor (MR) (Figure 1). In this design, some reaction products (e.g., H_2) are selectively extracted from the reaction medium via permeation through the membrane shifting the equilibrium and consequently increasing the conversion. Alternatively, the amount of catalyst for a desired conversion level can be reduced. For this reason, MRs have deserved considerable attention in the scientific literature.[2]

As mentioned, the H_2 removal can be performed by using selective dense membranes of Pd or its alloys. To decrease the cost and to increase the permeation fluxes, composite membranes become an alternative. These membranes present a selective metallic layer on a substrate of high porosity and low resistance to flow.[3–5]

Several authors have developed mathematical models to evaluate the advantages of using MRs for the WGSR.[5–7] However, in most of these works, the heat effects were neglected and the reactor operation was considered to be isothermal. This is a common assumption in MR modeling because it corresponds to the temperature measurements inside the reactor

Correspondence concerning this article should be addressed to D. O. Borio at dborio@plapiqui.edu.ar
Current address of Eduardo López: Institut de Tecniques Energetiques, Universitat Politecnica de Catalunya, Av. Diagonal 647, ed. Etseib, 08028 Barcelona, Spain.

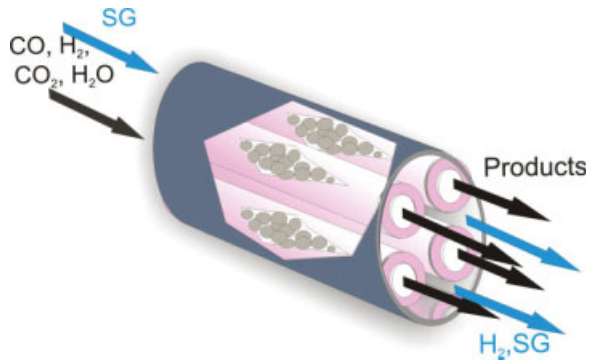

Figure 1. Scheme of the membrane reactor.

[Color figure can be viewed in the online issue, which is available at www.interscience.wiley.com.]

at laboratory scale due to the high ratio between the heat transfer area and the reactor volume. This condition may not be true when higher process scales are necessary; e.g., when several membrane tubes are installed in parallel within a shell where the sweep gas is circulated. Here, the usual assumption of isothermal MR should be reviewed and the heat effects taken into account.[8–11] To this end, Kokou et al.[9] presented a mathematical model considering mass dispersion for the simulation of an adiabatic full-scale membrane reactor for the WGSR. Chiappetta et al.[12] simulated the behavior of a nonisothermal membrane reactor for the WGSR by means of a two-dimensional mathematical model. The authors presented a theoretical sensitivity analysis of different variables (sweep gas flow rate, temperature, and pressure) on the performance of a membrane reactor.

In both of the works mentioned earlier, the nonisothermal membrane reactors were only operated in a cocurrent mode, i.e., with the sweep gas and the reactive mixture streams flowing in parallel. It is worth mentioning that the countercurrent operation in MRs have been studied by Basile et al.[7] but only under isothermal conditions. Here, the comparison of flow configurations refers to the analysis of the driving force to remove the hydrogen from the product stream. Brunetti et al.[13] analyzed the effect of increasing the operating pressure (i.e., driving force) on a MR without sweep gas by means of a 1D pseudohomogenous model under cocurrent mode.

The countercurrent operation could have an impact not only on the hydrogen removal rate but also on the heat transfer rate with the sweep gas. However, it is well known that the heat feedback phenomenon, typical of the countercurrent configuration, can lead to steady-state multiplicity and instability conditions in fixed bed reactors. The steady-state multiplicity of countercurrently cooled tubular reactors has been extensively studied.[14,15] To our knowledge, stability analyses of MRs operated in a countercurrent mode have not been reported yet.

In this work, the performance of a MR for the WGSR is simulated and compared with that of a fixed-bed reactor (CR) for nonisothermal nonadiabatic conditions. For both reactors, the influence of different operating conditions on the stability and performance is analyzed for two different configurations of the sweep gas flow through the shell: cocurrent and countercurrent.

Mathematical Model

Figure 1 shows a scheme of the membrane reactor under study. It consists of several concentric tubes assembled in an adiabatic shell where the sweep gas flows. The membrane consists of a dense Pd layer on a porous ceramic support. The catalyst is packed in the inner side of the tubular membranes.

A 1D pseudo-homogeneous mathematical model has been selected to simulate the steady-state operation of the reactors. The model is subject to the following assumptions:

(a) Mass and heat transfer dispersion effects are neglected.

(b) Negligible mass and heat-transfer resistances between catalyst and process gas.

(c) Isobaric conditions on the permeate side.

(d) Infinite selectivity for the membrane (H_2 is the permeation gas).

(e) The shell is adiabatic.

The Langmuir-Hinshelwood kinetic model proposed for the WGSR by Podolski and Kim[16] is considered.

From these assumptions, the governing equations for the reaction and permeation sides are given below:

Reaction Side (catalyst tubes):

Mass Balances

$$\frac{dF_{CO}}{dz} = A_T r_{CO} \rho_B \tag{2}$$

$$\frac{dF_{H_2}}{dz} = A_T(-r_{CO})\rho_B - \pi d_{te} J_{H_2} \tag{3}$$

Energy Balance

$$\frac{dT}{dz} = \frac{A_T \rho_B (-r_{CO})(-\Delta H_r) - \pi d_{ti} U (T - T_P)}{\sum_{j=1}^{N} F_j C_{pj}} \tag{4}$$

Permeation Side (shell):

Mass Balances

$$(\pm)\frac{dF_{H_2,P}}{dz} = \pi\, d_{te} n_t J_{H_2} \tag{5}$$

$$(\pm)\frac{dF_{SG,P}}{dz} = 0 \tag{6}$$

Energy Balance

$$(\pm)\frac{dT_P}{dz} = \frac{\pi d_{te} n_t (T - T_P)}{\sum_{j=1}^{2} F_{j,P} C_{pj}} \left[J_{H_2} C_{pH_2} + U \frac{d_{ti}}{d_{te}} \right] \tag{7}$$

$$\begin{cases} +, & \text{cocurrent flow} \\ -, & \text{countercurrent flow} \end{cases}$$

Boundary conditions:

Cocurrent flow

$$\text{at } z=0 \begin{cases} F_j = F_{jo} \quad \text{for} \quad j=1,2\ldots,N \\ T = T_0; T_P = T_{Pi} \\ F_{H_2,P} = 0; F_{SG} = F_{SG,i} \end{cases} \tag{8}$$

Countercurrent flow

$$\text{at } z=0 \begin{cases} F_j = F_{jo} \quad \text{for} \quad j=1,2\ldots,N \\ T = T_0 \end{cases} \tag{9}$$

$$\text{at } z=L \begin{cases} F_{H_2,P} = 0; F_{SG} = F_{SG,i} \\ T_P = T_{P,i} \end{cases} \tag{10}$$

The hydrogen permeation flux through the membrane is quantified using the Sievert's Law[17]:

$$J_{H_2} = \frac{Q_0 e^{(-E_P/RT_g^r)}}{\delta}\left[\sqrt{p_{H_2}^r} - \sqrt{p_{H_2}^p}\right] \tag{11}$$

where δ is the membrane thickness and $p_{H_2}^r$ and $p_{H_2}^p$ are the hydrogen partial pressures on the reaction and permeation sides, respectively.

The use of low-diameter tubes (0.3″) supports the assumption of a 1D model. However, the phenomenon of hydrogen permeation through the membrane tends to intensify the temperature gradients along the radial coordinate in comparison with those of a conventional fixed-bed reactor.[12] Therefore, in future contributions, it would be worth analyzing the membrane reactor performance and stability by using a 2D model.

The overall-heat transfer coefficient (U) is evaluated using an equation which was proposed by Abo-Ghandera et al.[18] for a MR in the dehydrogenation of ethylbenzene to styrene coupled with hydrogenation of nitrobenzene to aniline.

The wall heat-transfer coefficient (α_w) and the effective radial heat conductivity (k_{er}) are calculated using the correlations proposed by Dixon and Cresswell.[19] The overall convective heat transfer coefficient in a fixed bed reactor (α_i) is estimated following the guidelines reported by Dixon[20] and the heat-transfer coefficient corresponding to the shell side (α_e) was evaluated from Kern[21] equation. The thermal conductivity of the support ($\lambda_{\alpha Al_2O_3}$) and the Pd membrane (λ_{pd}) were obtained from literature, Hussain et al.[11] and Incropera and DeWitt,[22] respectively.

The CR is modeled by considering the hydrogen flow through the membrane ($J_{H_2} = 0$) equal to zero.

The differential equations that represent the model were integrated by means of a Gear algorithm. According to the boundary conditions, the equations for the countercurrent scheme constitute a boundary-value problem, which was solved iteratively by means of the shooting method. To satisfy the boundary conditions at $z = L$ (F_{H_2P}, $= 0$ and $T_P = T_{P,i}$; see Eq. 10), the hydrogen flowrate (F_{H_2P}) and the permeate temperature (T_P) at the axial position $z = 0$ were chosen as iteration variables. A Quasi-Newton algorithm was selected to reach convergence.

Table 1. Geometric Parameters and Operating Conditions Used to Simulate the MR and the CR

L	150 mm*	$F_{SG,i}$	20.7 L(STP)/min
d_{ti}	8 mm*	F_{T_0}	9.58×10^{-3}mol/s
d_{te}	13.4 mm*	CO, %	7.97**
n_t	30	CO_2, %	10.99**
W	9.64 g*	H_2, %	43.48**
δ	60 μm*	H_2O, %	31.88**
P_o	1 atm*	CH_4, %	5.68**

*Ref. 5.
**Ref. 1.

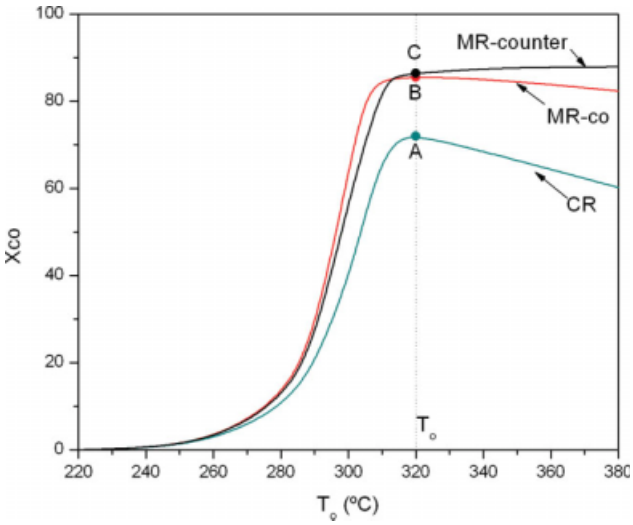

Figure 2. Outlet CO conversion vs. process gas inlet temperature for CR (J_{H_2} = 0) and MR (cocurrent and countercurrent configuration).

Adiabatic operation ($U = 0$). $T_{P,i} = 290$°C. [Color figure can be viewed in the online issue, which is available at www.interscience.wiley.com.]

Results and Discussion

The influence of different parameters and operating conditions on the CO conversion and the stability of the reactors (MR and CR) are analyzed in this section.

The design parameters and operating conditions used in the simulations are given in Table 1.

Effect of the heat transfer coefficient

The operation of both reactors (MR and CR) is analyzed first under adiabatic conditions, i.e., the global heat coefficient is set to zero ($U = 0$) and the only source of heat exchange between both sides is the permeating hydrogen flow.

Figure 2 shows outlet CO conversions as a function of inlet temperatures for both reactors. The lower curve (corresponding to the CR) is well known: the CO conversion increases first due to a kinetic effect and then decreases according to the equilibrium limitations. These restrictions are overcome in the upper curves, i.e., higher conversions are obtained in the MR for both flow configurations. The countercurrent scheme leads to slightly higher conversions than the cocurrent arrangement, provided the reaction is ignited. To compare the heat effects for the studied schemes, Figure 3 shows the corresponding conversion-temperature trajectories for the operating points labeled A–C in Figure 2. The three lines are represented by the following relationship:

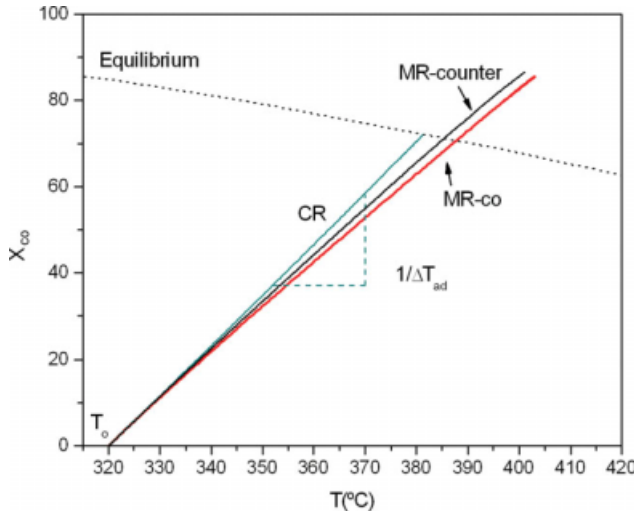

Figure 3. Conversion-temperature trajectories for CR ($J_{H_2} = 0$) and MR (cocurrent and countercurrent configurations).

$T_0 = 320°C$. Adiabatic operation. $T_{P,i} = 290°C$. (Conditions A, B, and C of Figure 2). [Color figure can be viewed in the online issue, which is available at www.interscience.wiley.com.]

$$\frac{dx_{CO}}{dT} = \frac{1}{\Delta T_{ad}}\left(\frac{F_T}{F_{T_0}}\right) \tag{12}$$

As it can be seen, the trajectories for the MR shift to the right with respect to the classical straight line (slope = ΔT_{ad}^{-1}) of the CR, resulting in a higher temperature rise in the MR than in the CR. This behavior is due to two reasons: (1) the total amount of heat being generated is higher (higher CO conversions) and (2) the total molar flowrate in the reaction side (F_T) diminishes along the reactor length as a consequence of the continuous H_2 permeation. That is, the ratio (F_T/F_{T_0}) in the right hand side of Eq. 12 decreases continuously in the MR while it is equal to unity in the CR. For the application of the WGSR considered in the present contribution, this effect could become relevant because the Pd membrane permeates not only the H_2 being generated by the reaction but also the H_2 coming from the steam reformer (see the feed composition in Table 1).

The membrane reactor analysis is extended to nonadiabatic conditions for two different flow configurations of the gas flowing through the shell: cocurrent and countercurrent. Figure 4 shows the exit CO conversion as a function of the

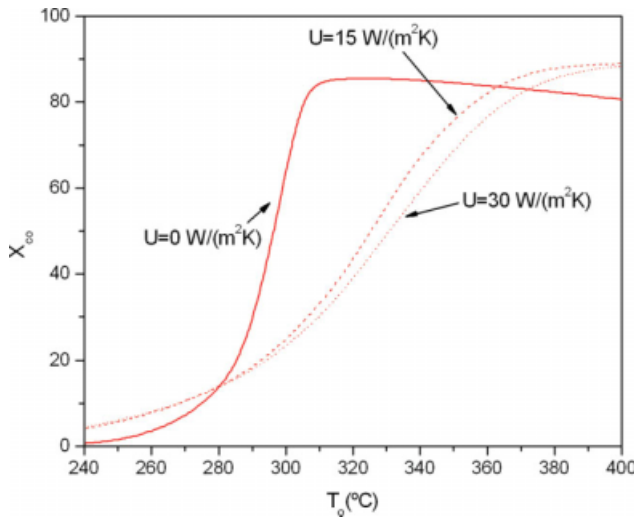

Figure 4. Outlet CO conversion vs. inlet temperature for MR (cocurrent configuration).

Adiabatic and nonadiabatic operation for different values of U. $T_{P,i} = 290°C$. [Color figure can be viewed in the online issue, which is available at www.interscience.wiley.com.]

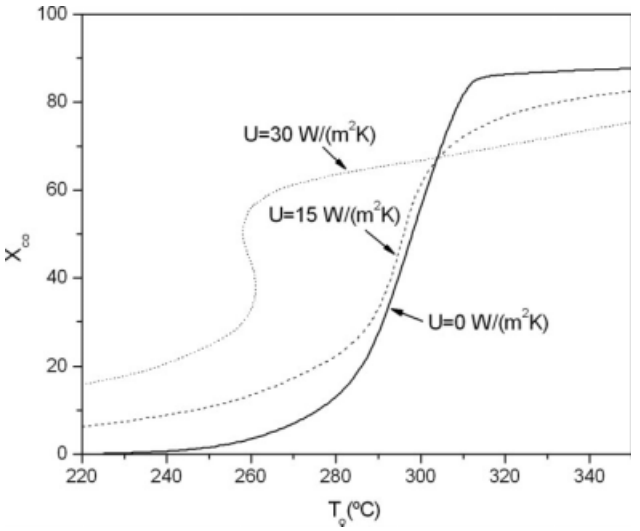

Figure 5. Outlet CO conversion vs. inlet temperature for MR (countercurrent configuration).

Adiabatic operation and nonadiabatic operation for different values of U. $T_{P,i} = 290°C$.

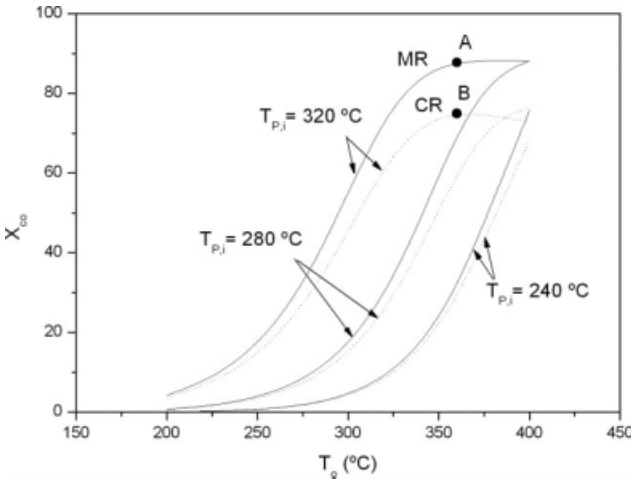

Figure 6. Outlet CO conversion vs. inlet temperature for different permeate inlet temperatures (cocurrent scheme).

MR(—); CR (---), U calculated.

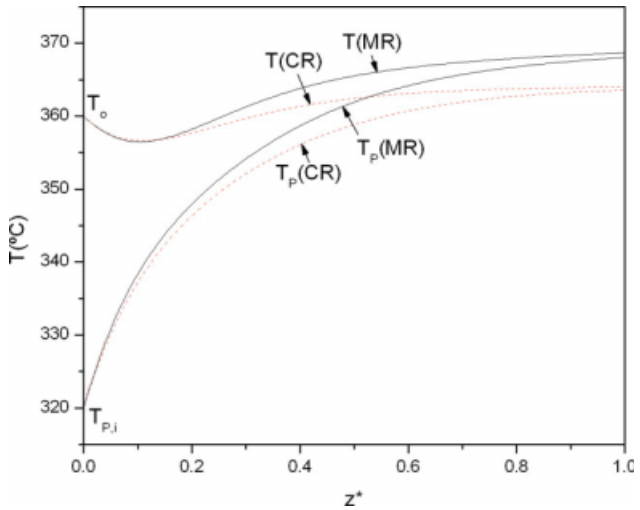

Figure 7. Axial temperature profiles for tube (T) and shell (T_P) sides MR(—); CR (---).

$T_0 = 360°C$, $T_{P,i} = 320°C$, U calculated. (Operating conditions A and B of Figure 6). [Color figure can be viewed in the online issue, which is available at www.interscience.wiley.com.]

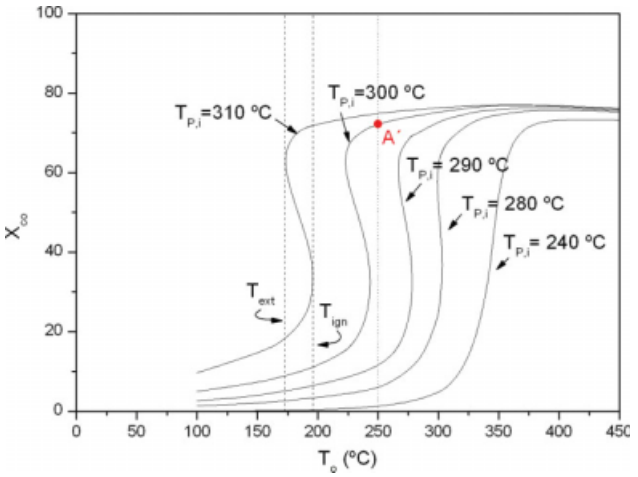

Figure 8. Outlet CO conversion vs. inlet temperature for different permeate inlet temperatures in the CR.

Countercurrent scheme, $Q_{SG,i} = 20.7$ L(STP)/min. [Color figure can be viewed in the online issue, which is available at www.interscience.wiley.com.]

inlet temperature for different values of the overall heat transfer coefficient (U) for cocurrent operation. As it can be seen, as U increases the curves shift to the right leading to higher ignition temperatures. In fact, to obtain high conversions, higher inlet temperatures are required due to the cooling effect produced by the sweep gas at the reactor entrance. However, the nonadiabatic MR leads to lower temperature rises inside the catalyst tubes.

When the countercurrent scheme is chosen, typical S-shaped curves are obtained (Figure 5), as a consequence of the heat feedback toward the reactor inlet. Therefore, the reactor could be operated under three different steady-states for the same inlet temperature. In this case, the curves shift to the left (Figure 5) as U increases, which indicates that the reaction ignites at lower inlet temperatures. As higher values of U are selected, the heat transferred to the sweep gas increases. When countercurrent operation is considered, the mean temperature of the sweep gas for lower values of the axial coordinate increases and so does the preheating effect over the incoming process gas.

Influence of the inlet sweep gas temperature

The steady-state behaviors of both reactors (MR and CR) for the cocurrent flow configuration are shown in Figure 6 for different sweep gas inlet temperatures. As expected, the cocurrent flow scheme does not present steady-state multiplicity in any of both reactor designs. The ignition temperature diminishes as the sweep gas inlet temperature increases. For the analyzed operating conditions, the MR exhibits higher outlet conversions and lower ignition temperatures than the CR. This aspect can be explained by means of Figure 7, in which the axial temperature profiles (T and T_P) for both reactors are presented (conditions A and B of Figure 6). The H_2 permeation through the membrane in the MR leads to higher conversions and therefore to higher axial temperatures. Another characteristic of the MR that contributes to increasing the permeate temperature is a convective flux ($J_{H_2}C_{PH_2}$) from the reaction side to the shell side. Besides, the overall heat transfer coefficient calculated for the MR is higher than in the CR for all axial positions (dominating effect of higher α_e due to higher flows in the shell side).

The analysis of the steady-state behaviors of both reactors (MR and CR) for the countercurrent flow configuration is also presented. In Figure 8, the outlet conversion is plotted against the inlet temperature for different permeate inlet temperatures ($T_{P,i}$) for the CR. For the chosen operating conditions, the CR presents instability for $T_{P,i} > 280°C$. As mentioned, the multiplicity of steady-states occurs as a consequence of heat feedback occurring in the countercurrent

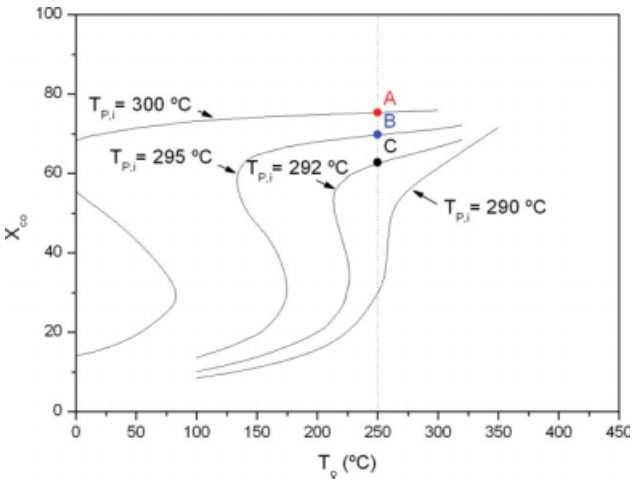

Figure 9. Outlet CO conversion vs. inlet temperature for different permeate inlet temperatures in the MR.

Countercurrent scheme, $Q_{SG,i} = 20.7$ L(STP)/min. [Color figure can be viewed in the online issue, which is available at www.interscience.wiley.com.]

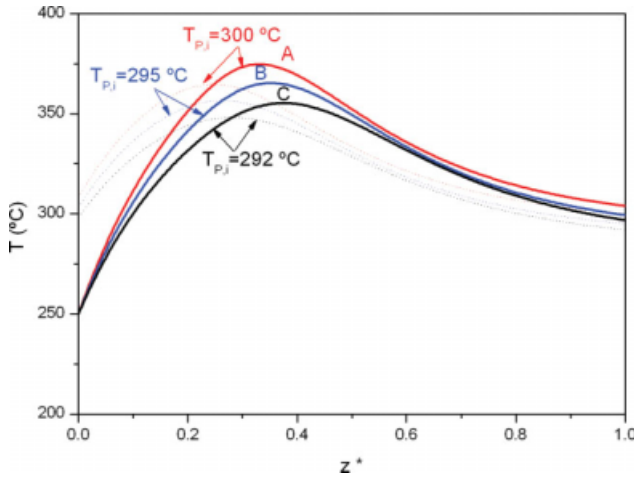

Figure 10. Axial temperature profiles of reaction (—) and permeation (---) sides in the MR corresponding to operating points A, B, and C of Figure 9.

T_0 = 250°C, $T_{P,i}$ = 292, 295, and 300°C, $Q_{SG,i}$ = 20.7 L(STP)/min. [Color figure can be viewed in the online issue, which is available at www.interscience.wiley.com.]

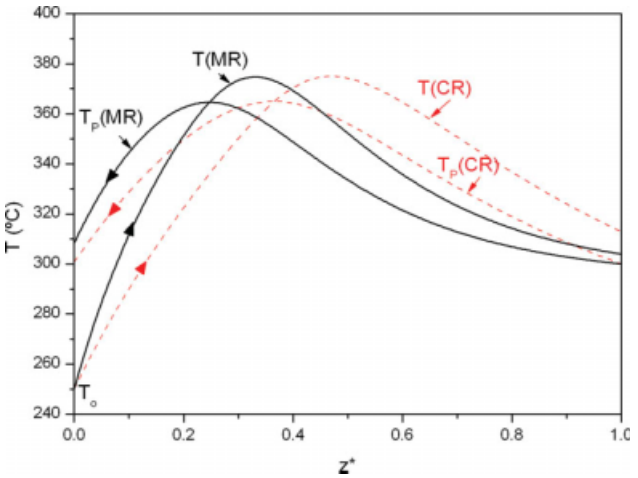

Figure 12. Axial temperature profiles for CR and MR corresponding to points A′ and A of Figures 8 and 9, respectively.

[Color figure can be viewed in the online issue, which is available at www.interscience.wiley.com.]

configuration. Both the ignition temperature (T_{ing}) and the extinction temperature (T_{ext}) are highlighted (with dashed lines) for $T_{P,i}$ = 310°C.

Figure 9 reports a similar analysis but for the MR. As shown, the variations of outlet CO conversions in the MR are larger than in the CR when $T_{P,i}$ increases for the selected operating conditions. Above $T_{P,i}$ = 292°C, the S-shaped curves are extremely sensitive with respect to the inlet temperature of the permeate stream. This behavior could be analyzed from the axial temperature profiles presented in Figure 10 at T_0 = 250°C and for different permeate inlet temperatures ($T_{P,i}$) (corresponding to operating points A, B, and C of Figure 9). As it can be seen, even when a small modification of the permeate inlet temperature occurs (3 and 5°C), a noticeable variation on the temperature profiles of both the reaction and shell sides is achieved.

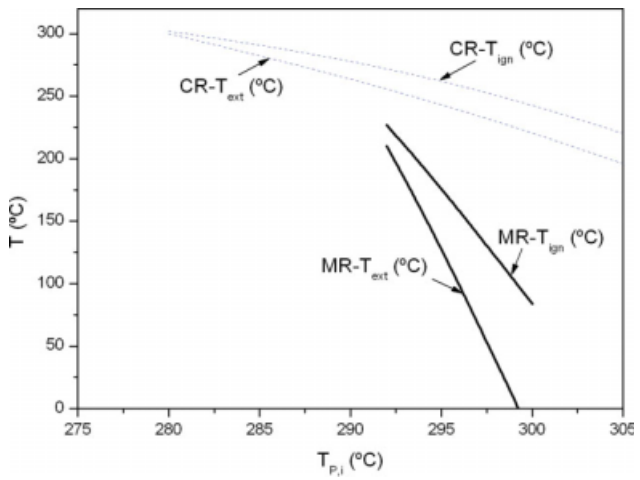

Figure 11. Ignition and extinction temperatures vs. permeate inlet temperature for CR (---) and MR (—).

$Q_{SG,i}$ = 20.7 L(STP)/min. [Color figure can be viewed in the online issue, which is available at www.interscience.wiley.com.]

When $T_{P,i}$ increases, the temperature profiles shift up due to a slight augmentation in the heat transfer coefficient and the H_2 flow from the reaction side to the permeate side. This hot H_2 flux contributes to increase the permeate temperature in z^* ~0.3 and thus to increasing the heat flux toward the reaction side in the first portion of the reactor ($z^* < 0.3$). Besides, high temperatures lead to an augmentation of the H_2 permeation and therefore of the CO conversion.

If the permeate inlet temperature is reduced, for example from 292 to 290°C, the reaction is blown out (see Figure 9) and the axial temperature profile does not present a maximum.

To analyze the different behaviors related to the multiplicity of steady-states between CR and MR designs, both the ignition (T_{ing}) and extinction (T_{ext}) temperatures are plotted in Figure 11 as a function of the permeate inlet temperature ($T_{P,i}$). This information is obtained from Figures 8 and 9 for each ($T_{P,i}$).

As shown in Figure 11, the steady-state multiplicity zone begins at a lower $T_{P,i}$ in the CR than in the MR and consequently the CR presents a cusp point ($T_{ign} = T_{ext}$) for a lower $T_{P,i}$. Therefore, for the selected operating conditions, the MR ignites at a lower inlet temperature. To explain the differences between the MR and the CR, the axial temperature profiles for $T_{P,i}$ = 250°C are presented in Figure 12 for the CR and the MR (point A′ and A of Figures 8 and 9, respectively). For the same conditions, the hydrogen permeation in the MR leads to higher outlet CO conversion and, consequently, to higher temperatures than in the CR. The different behaviors of the MR and the CR could not only be due to the permeated H_2 but also due to the convective heat transfer. In fact, the heat transfer coefficient in the MR presents a higher axial variation in correspondence with the axial changes of temperatures and sweep gas flowrate. It is worth mentioning that the influence of the term $J_H C_{pH_2}$ in the energy balance of the sweep gas (Eq. 7) is small and represents ~5% of the total heat flux.

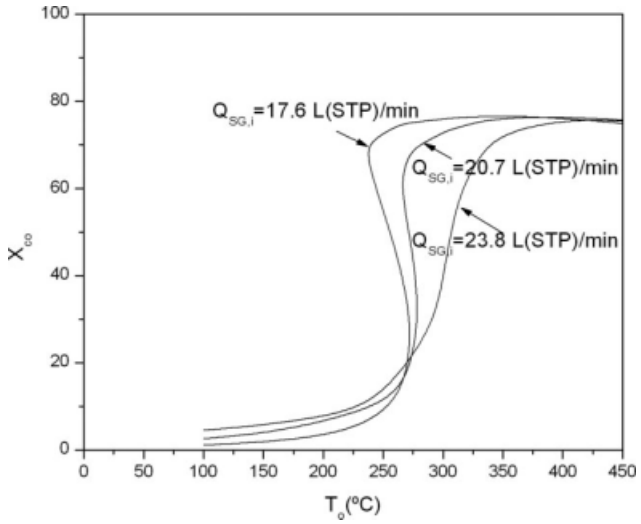

Figure 13. Outlet CO conversion vs. inlet temperature for different sweep gas inlet flowrates in the CR.

Countercurrent scheme, $T_{P,i} = 290°C$.

Influence of the sweep gas flowrate (Q_{SG})

The influence of the inlet sweep gas flowrate on the performance of the CR and MR is analyzed for the countercurrent configuration. Figures 13 and 14 show the outlet CO conversion as a function of the inlet temperature for $T_{P,i} = 290°C$ in the CR and the MR, respectively. As it can be seen, both reactors present multiplicity of steady-states for the operating conditions analyzed. Besides, the ignition temperatures are lower as the sweep gas flowrate increases. However, changes in the Q_{SG} lead to S-shaped curves more pronounced in the MR. As a result, the differences between the ignition and the extinction temperatures are higher in the MR. Just like it was observed in the analysis of the sweep gas inlet temperature (Figure 9), small changes in the Q_{SG} could lead to very different steady-state conditions even though the other operating variables are not modified, points D and E of Figure 14. The axial temperature profiles corresponding to the operating conditions of points D and E of Figure 14 are presented in Figure 15. As the sweep gas flowrate diminishes, the outlet permeate temperature (at $z = 0$) is higher leading to superior heat feedback toward the entrance of the reactor and to higher instability.

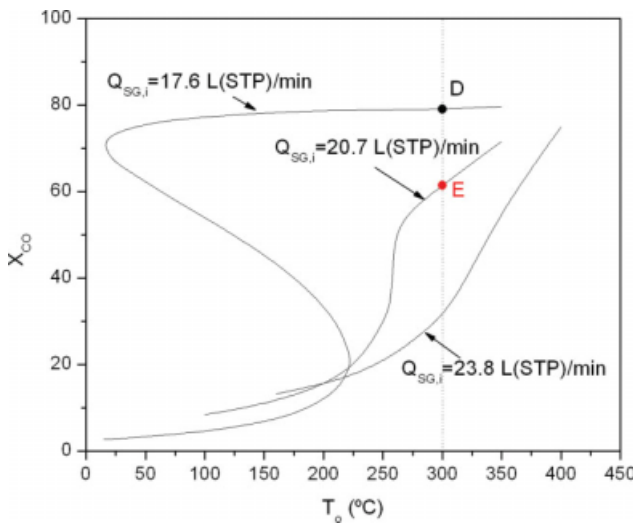

Figure 14. Outlet CO conversion vs. inlet temperature for different sweep gas inlet flowrates in the MR.

Countercurrent scheme, $T_{P,i} = 290°C$. [Color figure can be viewed in the online issue, which is available at www.interscience.wiley.com.]

Conclusions

When adiabatic conditions are selected, the total temperature rise inside the reactor is higher for the MR due to the higher conversions achieved and the reduction of the total gas flowrate in the reaction side as a consequence of the hydrogen permeation. When nonadiabatic conditions are considered, the proper selection of the operating conditions and the configuration of the sweep gas flow become determining to avoid undesirable temperature rises over the catalyst and high parametric sensitivity.

A comparative analysis of the stability in the CR and in the MR has demonstrated that the countercurrent operation shows multiplicity of steady-state for certain operating conditions. The stability of both reactors (CR and MR) increases (i.e., the extinction temperature decreases) as the sweep gas flow and the inlet temperature decrease.

For all the operating conditions studied, the regions where the multiple steady-states occur are wider in the MR than in the CR. This high instability in the MR could be attributed to the hydrogen permeation through the membrane magnifying the thermal effects. The hydrogen permeation improves the CO conversion and generates a convective heat flux from the reaction side to the permeate side. The variation of the flow in both sides also leads to a higher global heat coefficient.

On the other hand, the cocurrent configuration does not exhibit steady-state multiplicity and leads to lower parametric sensitivity and more isothermal axial profiles, provided

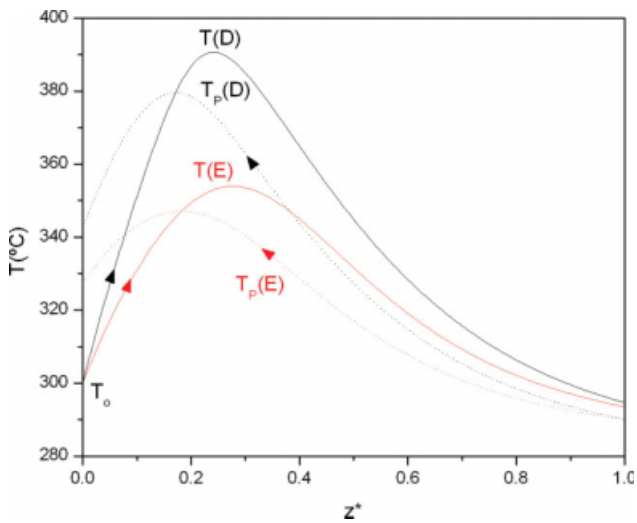

Figure 15. Axial temperature profiles for MR corresponding to points D and E of Figure 14.

[Color figure can be viewed in the online issue, which is available at www.interscience.wiley.com.]

that the inlet temperatures of the feed and the sweep gas are properly selected.

Acknowledgments

The authors acknowledge Universidad Nacional del Sur (UNS), Consejo Nacional de Investigaciones Científicas y Tecnológicas (CONICET), and Agencia Nacional de Promoción de Ciencia y Tecnología (ANPCyT) for the financial support.

Notation

A_T = cross sectional area of tubes, m^2
Cp_j = specific heat of component j, kJ/(mol K)
d_{te} = external tube diameter, m
d_{ti} = internal tube diameter, m
E_p = activation energy of the hydrogen permeability,J/mol
F = molar flow, mol/s
J_{H_2} = permeation flow of hydrogen, mol/(s m^2)
L = tube length, m
N = number of components (reaction side)
n_t = number of tubes
p_{H_2} = partial pressure of hydrogen, Pa
Q = volumetric flow, L/min
Q_0 = pre-exponential factor of the Sievert permeability coefficient, mol/(s m $Pa^{1/2}$)
r_{CO} = reaction rate, $mol_{CO}/(kg_{cat}$ s)
T = temperature, K
U = overall heat transfer coefficient, kJ/(s m^2 K)
W = catalyst mass, g
y = molar fraction
z = axial coordinate, m

Greek letters

δ = thickness of Pd film, m
ΔH_r = heat of reaction, kJ/mol
$\Delta T_{ad} = \frac{(-\Delta H_r)y_{co,i}}{\overline{C}_p}$ = adiabatic temperature rise
ρ_B = bed density, kg_{cat}/m^3

Subscripts

CO = carbon monoxide
H_2 = hydrogen
i = inlet
j = component j
T = total
0 = at the axial coordinate $z = 0$
L = at the axial coordinate $z = L$
P = at permeation side
SG = sweep gas

Acronyms

STP = standard temperature and pressure (0°C and 1 atm)

Literature Cited

1. Francesconi JA, Mussati MC, Aguirre P. Optimización del reactor WGS como componente del procesador de etanol para celdas PEM. In: *XX SICAT-Simposio Ibero-Americano de Catálise*, Brasil, Gramado, 2006.
2. Coronas J, Santamaría J. Catalytic reactors based on porous ceramic membranes. *Catal Today*. 1999;51:377–389.
3. Oklany JS, Hou K, Hughes R. A simulative comparison of dense and microporous membrane reactors for the steam reforming of methane. *Appl Catal A*. 1998;170:13–22.
4. Tosti S, Bettinali L, Violante V. Rolled thin Pd and Pd-Ag membranes for hydrogen separation and production. *Int J Hydrogen Energy*. 2000;25:319–325.
5. Criscuoli A, Basile A, Drioli E. An analysis of the performance of membrane reactors for the water-gas shift reaction using gas feed mixtures. *Catal Today*. 2000;56:53–64.
6. Basile A, Chiappetta G, Tosti S, Violante V. Experimental and simulation of both Pd and Pd/Ag for a water gas shift membrane reactor. *Sep Purif Technol*. 2001;25:549–571.
7. Basile A, Paturzo L, Galluci F. Co-current and counter-current modes for water gas shift membrane reactor. *Catal Today*. 2003;82:275–281.
8. Bratch M, Alderliesten P, Kloster R, Pruschek R, Haupt G, Xue E, Ross J, Koukou M, Papayannakos N. Water gas shift membrane reactor for CO_2 control in IGCC systems: techno-economic feasibility study. *Energy Conversion Manage*. 1997;38:159–164.
9. Koukou MK, Papayannakos N, Markatos NC. On the importance of non-ideal flow effects in the operation of industrial-scale adiabatic membrane reactors. *Chem Eng J*. 2001;83:95–105.
10. De Falco M, Di Paola L, Marrelli L, Nardella P. Simulation of large-scale membrane reformers by a two-dimensional model. *Chem Eng J*. 2007;128:115–125.
11. Hussain A, Seidel-Morgenstern A, Tsotsas E. Heat and mass transfer in tubular ceramic membranes for membrane reactors. *Int J Heat Mass Transfer*. 2006;49:2239–2253.
12. Chiappetta G, Clarizia G, Drioli E. Theoretical analysis of the effect of catalyst mass distribution and operation parameters on the performance of a Pd-based membrane reactor for water-gas shift reaction. *Chem Eng J*. 2008;136:373–382.
13. Brunetti A, Caravella A, Barbieri G, Drioli E. Simulation study of water gas shift reaction in a membrane reactor. *J Membr Sci*. 2007;306:329–340.
14. Luss D, Medellin P. Steady-state multiplicity and stability in a countercurrently cooled tubular reactor. In: *Proceedings of European Symposium on Chemical Reaction Engineering*, Amsterdam, Holland, 1972:B4-B47.
15. Eigenberger G. Stability and dynamics of heterogenous catalytic systems. *Int Chem Eng*. 1981;21:17–28.
16. Podolski WF, Kim YG. Modeling the water-gas shift reaction. *Ind Eng Chem*. 1974;13:415–421.
17. Barbieri G, Brunetti A, Granato T, Bernardo P, Drioli E. Engineering evaluations of a catalytic membrane reactor for the water gas shift reaction. *Ind Eng Chem Res*. 2005;44:7676–7683.
18. Abo-Ghandera NS, Gracea JR, Elnashaie SSEH, Lima CJ. Modeling of a novel membrane reactor to integrate dehydrogenation of ethylbenzene to styrene with hydrogenation of nitrobenzene to aniline. *Chem Eng Sci*. 2008;63:1817–1826.
19. Dixon AG, Cresswell DL. Theoretical prediction of effective heat transfer parameters in packed beds. *AIChE J*. 1979;25:663–676.
20. Dixon AG. An improved equation for the overall heat transfer coefficient in packed beds. *Chem Eng Process*. 1996;35:323–331.
21. Kern DQ. *Process Heat Transfer*, *1st ed*. New York: McGraw-Hill, 1950: Chapter 7.
22. Incropera FP, DeWitt DP. *Fundamentos de transferencia de calor*. México: Prentice Hall, 1999:Apéndice A.

Manuscript received Aug. 26, 2008, and revision received Mar. 23, 2009.